Biotechnology Progress
DOI 10.1002/btpr.2491



# CHO cells engineered for fluorescence read out of cell cycle and growth rate in real time

Short running title:
**A fluorescence read out for the growth rate**

Grischa Fuge[1]
Yaeseong Hong[1]
Kristoffer Riecken[2]
An-Ping Zeng[1]
Uwe Jandt[1*]

[1]Institute of Bioprocess and Biosystems Engineering, Hamburg University of Technology, Hamburg, Germany
[2]Research Department Cell and Gene Therapy, Department of Stem Cell Transplantation, University Medical Centre (UMC) Hamburg-Eppendorf, Hamburg, Germany
* Corresponding Author.

**Correspondence:** Dr. Uwe Jandt (Uwe.Jandt@TUHH.de). Institute of Bioprocess and Biosystems Engineering, Hamburg University of Technology, Hamburg, Germany

**Keywords:** Biosensor, Cell Cycle, FUCCI, Process Control, Process Parameter

**Abbreviations:**
**FUCCI**, Fluorescent Ubiquitination-based Cell Cycle Indicator system;


Received: Dec 22, 2016; Revised: Apr 08, 2017; Accepted: Apr 21, 2017

**Abstract**

For efficient production of recombinant proteins by mammalian cells in a bioreactor, optimal growth rates are required and represent the most important process parameter. We present the first successful attempt to monitor the growth behavior and cell cycle state of a mammalian production relevant cell line under bioreactor cultivation conditions up to 1.2 l, utilizing a fluorescent read-out without the need of additional staining or marking. For this purpose, we developed two new production relevant cell line derivatives (*CHO-K1 FUCCI CM* & *CHO-K1 FUCCI CN*) and corresponding analytical methods. The approach is easily scalable, applicable to mammalian recombinant protein production cell lines, and it allows for real-time monitoring using appropriate fluorescence probes. It is based on the Ubiquitination-based Cell Cycle Indicator (*FUCCI*) system developed by Miyawaki et al. CHO-K1 was chosen as a model cell line due to its close relationship to several production cell lines [1].

We defined a new process parameter $i_{red}$, a quantitative and numerically robust representation of the cell cycle distribution, and demonstrate it to be linearly correlated with the cell cycle state and inversely related to the real time growth rate. Detection of growth rate limitations is possible earlier than using cell-count based approaches. Analytics were compatible with bulk fluorescence methods, using a plate reader as well as a flow cytometer. For future real time applications in industry scale bioreactors we recommend the use of on-line or at-line fluorescence probes.

## 1 Introduction

Process control strategies of mammalian cell cultivations rely, amongst others, on the need to monitor the growth of viable cell mass and its variation in real time or close to real time. Conventionally, this data is derived from indirect measurements including oxygen uptake rate (OUR) as well as calculation of the growth rate (μ) from the variation of cell densities or biomass over multiple measurements taken at different time points [2].

Other studies suggested automated flow cytometer setups as means for process control [3,4]. The concept is based on the fact that the transition of cells from late G1 to S phase is tightly controlled by different aspects including growth factors and nutrient availability [5]. These approaches based on automated flow cytometry are inevitably connected to high

automatization and financial efforts, since they re-implement conventional staining procedures and rely on flow cytometer hardware.

Here we present, to our knowledge, the first concept to detect the growth behavior of mammalian production relevant cell lines in a real time feasible manner. For this purpose two novel derivatives (*CHO-K1 FUCCI CM* & *CHO-K1 FUCCI CN*) were generated. The approach utilizes the Fluorescent Ubiquitination-based Cell Cycle Indicator (*FUCCI)* system [6,7], which was already implemented for a broad variety of applications including animal models [8–11] as well as drug screening [12,13]. Various elaborate studies utilized FUCCI to reveal the chemo sensitivity and resistance of cells to anti cancer drugs [14], influenced by their cell cycle state and growth dynamics [15], *in vivo* location [15] and 2D vs. 3D *in vitro* histoculture. Additionally, synergistic effects with agents like caffeine [16], herbal mixtures [17] and recombinant methioninase (rMETase) [18].

Furthermore, a CHO-DG44 derivative with FUCCI was used in a study elucidating the role of homologous recombination proteins in cell cycle regulation [19]. However, no project targeting real time compatible detection of the growth rate was reported, yet [20].

Potential applications are manifold, as real-time detection of the cell cycle distribution and growth behavior may pave the way for novel optimization strategies including, but not limited to, circumventing limitations and optimized feeding. Furthermore it holds potential for the monitoring of bioreactor heterogeneity, for example by using an array of fluorescent probes.

This study consists of three consecutive stages. First, two novel cell line derivatives of the CHO-K1 cell lines were generated. In the second part, the process parameter $i_{red}$ was defined and validated, representing a normalized and robust fluorescence intensity. This parameter was demonstrated to be a reliable indicator for the cell cycle distribution. In the third section, it was further shown that $i_{red}$ is negatively related to the growth rate ($\mu$). This holds true for different methods of fluorescence detection and cell culture systems as demonstrated by a monitored repeated batch process.

## 2 Materials and Methods

### 2.1 Generation of two novel FUCCI cell line derivatives

#### Mammalian cell line and medium

The *CHO-K1* cell line was adapted to growth in suspension and later generously donated by Prof. Dr. Thomas Noll (Cell Culture Technology Group, University Bielefeld, Germany). Cultures of the initial *CHO-K1* as well as the derivatives *CHO-K1 FUCCI CM* and *CHO-K1 FUCCI CN* were maintained in suspension in complete chemically-defined, animal-component-free and protein-free CHOMACS CD Medium (Miltenyi Biotec GmbH, Bergisch Gladbach, Germany), supplemented with 4 mM glutamine, without antibiotics. A constant humidified atmosphere of 37°C and 5% CO2, as well as continuous shaking (200 rpm) were kept throughout the cultivation. Erlenmeyer baffled cell culture flasks (125 ml: Type 431405, 250 ml: Type 431407; Corning, New York, USA) were used with culture volumes of 40 ml and 80 ml, respectively.

**FUCCI plasmids**

The FUCCI plasmids containing a third generation lentiviral SIN vector expressing different cell cycle specific fluorescent proteins, plasmid C: mKO2-hCdt1(30/120); M: mVenus-hGeminin(1/110) and N: mVenus-hGeminin(1/60), were generous gifts from the Group of Dr. A. Miyawaki (Laboratory for Cell Function Dynamics, RIKEN Brain Science Institute, Saitama, Japan).

**Lentiviral transduction**

Production of lentiviral particles was described earlier [21] and protocols are available online (www.LentiGO-Vectors.de). The transduction of suspension culture adapted CHO-K1 cells was done in a 24 well plate with 50,000 cells in 500 µl CHOMACS CD Medium (Miltenyi Biotec GmbH, Bergisch Gladbach, Germany) including 4 mM glutamine, per well. For two double transductions with the combinations of C and M [mKO2-hCdt1(30/120) and mVenus-hGeminin(1/110)] or C and N [mKO2-hCdt1(30/120) and mVenus-hGeminin(1/60)], 30 µl of each vector containing supernatant was used, resulting in 14% or 22% of labelled cells, respectively, as determined by flow cytometry after four days. In accordance with the legal framework cells were classified as S1 one week post transduction. Please note that actual transduction efficiencies cannot be measured exactly by flow cytometry, since the fluorescent proteins are only expressed in certain cell cycle states. Thus, the transduction rates will be underestimated by flow cytometry.

**Life cell sorting and flow cytometry**

Life cell sorting was conducted using a *FACSAria IIIu* (Becton Dickinson, Franklin Lakes, NJ, USA). Cells were sorted for highly positive red cells ("PE-Texas Red-A": 561 nm laser, 600 nm mirror, 610/20 nm filter) and expanded in culture for two weeks. Subsequently, those cells were sorted for highly positive green cells ("Alexa Fluor 488-A": 488 nm laser, 525 nm mirror, 543/22 nm filter) and expanded again. Verification measurements were conducted with an *LSRFortessa* flow cytometer ("Alexa Fluor 488-A": 488 nm laser, 505 nm LP filter, 530/30 nm BP filter; "PE-Texas Red": 561 nm laser, 600 nm LP filter, 610/20 nm BP filter).

## 2.2 The fluorescence ratio $i^n_{red}$ as read out for cell cycle distribution

**Cultivation**

Cell culture was performed using *CHO-K1 FUCCI CN* as described above. Inoculation densities and culture volumes were calculated to yield 200 Mio exponentially growing *CHO-K1 FUCCI CN* cells at the time of elutriation.

**Elutriation**

Counter flow elutriation was employed to generate fractions of cells with different cell cycle distributions. The method was published earlier [22], here it was used in an optimized version. For each experiment 200 Mio *CHO-K1 FUCCI CN* cells of exponentially growing cultures were separated at 1.800 rpm using flow rates of 5-50 ml/min. After separation, cells were parted from the elutriation buffer (PBS) by centrifugation (5 min at 119 g), split and subjected to the different flow cytometry protocols.

**Storage of cells**

For later analysis, cells were pelleted by centrifugation (3 min at 300 g) and resuspended in 70% EtOH at -20°C before they were stored at -20°C.

**Quantification of normalized FUCCI fluorescence with flow cytometry**

Analysis of FUCCI fluorescence was conducted by measuring viable cells, directly after sampling and washing or after elutriation, respectively, on a *CytoFlex* flow cytometer (Beckman Coulter, Brea, CA, USA). Prior to each experimental series, but at least once a

week, quality control was conducted following the manufacturers guidelines. Compensation settings (FITC - 24% PE; PE – 42.5% FITC) were applied to correct for crosstalk. Dead cells and doublets were excluded by gating. Subsequently, mVenus ("FITC-A": 488 nm laser, 525/40 nm filter, gain 50) and mKO2 fluorescence ("mKO2-A": 488 nm laser, 585/42 nm filter, gain 50) thresholds for fluorescence protein expression were defined, based on the direct comparison of *CHO-K1 FUCCI CN* (positive control) and *CHO-K1* cells (negative control). For mVenus, all cells within channel numbers above $2 \cdot 10^4$ were defined as positive. For mKO2, the corresponding value was $10^4$. These gates were kept constant for all samples. The total number of cells in these gates ($mKO2^n$ and $mVenus^n$, respectively) as well as the mean value of the gates ($mKO2^{mean}$ and $mVenus^{mean}$, respectively) were exported to CSV files in order to calculate the two normalized different $i_{red}$ values as follows:

$$i_{red}^{n}[\%] = \frac{mKO2^n}{mKO2^n + mVenus^n}$$

**Equation 1**

$$i_{red}^{nmean}[\%] = \frac{mKO2^n \times mKO2^{mean}}{mKO2^n \times mKO2^{mean} + mVenus^n \times mVenus^{mean}}$$

**Equation 2**

**Quantification of normalized FUCCI fluorescence with plate reader**

Measurements were conducted in a combined manner after finishing each biological experiment. Up to that point all cell samples were stored in 70% EtOH at -20°C. Of each sample, 200 µl were directly transferred into separate wells of black, flat bottom plates (Type 655076; Greiner Bio-one, Kremsmünster, Austria). In parallel the same volume of 70% ethanol was used as blank. Fluorescence intensities (I) were measured using a *Safire 2* plate photometer (Tecan, Männedorf, Switzerland). According to the fluorescence properties of mKO2 and mVenus [23], the following filter configurations were chosen to avoid crosstalk: mVenus Ex. 510 nm, Em. 533 nm; mKO2 Ex. 546 nm, Em. 571 nm. All: Bandwidths 10 nm, integration time 40 µs, Number of reads 20, Mode: *High sensitivity*, *manual Z axis* value 6000 µm. The *gain* value for each measurement value was determined using the *optimal gain* function for both fluorophores, prior to each measurement. The lower resulting *gain* value was manually set for mVenus and mKO2 measurement. The $i_{red}^{PR}$ value was calculated using the following equation:

$$i_{red}^{PR}[\%] = \frac{mKO2^{I} - mKO2^{\overline{I\ background}}}{mKO2^{I} - mKO2^{\overline{I\ background}} + mVenus^{I} - mVenus^{\overline{I\ background}}}$$

**Equation 3**

**Quantification of cell cycle distribution using DNA staining**

Directly prior to analysis, cells from storage (70% EtOH at -20°C, see above) were pelleted (3 min at 300 g), the EtOH was removed and cells were stained in 500 µl PBS containing 10 µg/ml Hoechst33342 and 0.1% Triton X-100 for 30 min at room temperature. The DNA-amount was detected using Hoechst33342 fluorescence ("PB450-A": 405 nm laser, 450/45 nm filter, gain 12). Data processing was conducted using the KALUZA Analysis 1.3 Software (Beckman Coulter, Brea, CA, USA). The gating strategy was designed to include dead cells, since all cells were expected to be dead as a result of the EtOH sample preparation, but exclude doublets. Finally, DNA histogram data was exported as CSV files and subjected to analysis by a Microsoft Excel (Microsoft, Redmond, CA, USA) script. Its function is as follows: (1) Find the first peak, corresponding to G1, (2) find the second peak, corresponding to G2/M peak, (3) normalize the distance between the two peaks, as they can deviate from the ideal unit distance, (4) calculate the G1 [%] based on fixed ranges around the found peaks, using the normalized distance. All distances were calculated in "channel numbers" of the histogram. In case of only one dominant peak (e.g. the first fractions, high G1), the ranges for the G1 and G2 peak were determined manually to avoid artifacts.

**Correlation of $i_{red}^{n}$ and G1 [%]**

The $i_{red}^{n}$ values of two elutriation experiments (biological replicates) were plotted against their corresponding G1 [%] values. The data was fitted using linear regression.

## 2.3 Relationship of the total fluorescence ratios ($i_{red}^{nmean}$ and $i_{red}^{PR}$) with the growth rate (µ) in shaking flask and VSF2000 bioreactor cultivations

### 2.3.1 Shaking flask based experiments

**Batch cultivations**

Cell culture was performed using *CHO-K1 FUCCI CM* and *CHO-K1 FUCCI CN* as described above. Initial cell densities were 0.8 Mio/ml.

**Glutamine depletion and feed experiments**

Cultivation was conducted in consecutive steps to yield varying L-glutamine concentrations. The preculture (4 mM L-glutamine) was cultured for 21 h, subsequently two cultures of different media composition were generated: "+Gln" including 4 mM L-glutamine, "-Gln" without L-glutamine. 29 h post limitation, the"-Gln" culture was split again, half of it was supplemented with 4 mM L-glutamine, and the rest remained glutamine depleted.

**Assessment of cell densities, viabilities and growth rate (μ)**

Viable cell densities c(t) and viabilities were assessed using an *Improved Neubauer* Chamber (BRAND, Wertheim, Germany) approach. The comparably high error of this method in combination with the strong error propagation of classical growth rate calculation was minimized using a Gaussian low-path filter [24] with a filter width of σ=12 h. Using the herewith obtained equally-sampled (with time step Δt) and filtered viable cell densities c'(t), the corresponding apparent growth rates μ were classically approximated as:

$$\mu\left(t+\frac{1}{2}\Delta t\right) \approx \frac{\ln\left(\frac{c'(t+\Delta t)}{c'(t)}\right)}{\Delta t}$$

**Equation 4**

**2.3.2 VSF 2000 bioreactor based experiments**

**Glutamine depletion and feed experiments**

A *VSF2000* bioreactor (BioEngineering, Wald, Switzerland) was used with *CHO-K1 FUCCI CN* and actively controlled parameters: pH 7.4, 37°C. DO was maintained at a minimum of 30% air oxygen saturation; one exception was a limited period of oxygen limitation (<10% air oxygen saturation, ranging from t~59h to t~66h post bioreactor inoculation) to investigate the responses of $i_{red}^{nmean}$ and $i_{red}^{PR}$ in such limitation. The period of 7 hours was chosen as a

compromise to give the oxygen limitation a sufficient period to take effect, while not overlaying the entire cultivation. The initial volume was 1.2 l, at the time of inoculation the CHOMACS CD Medium (Miltenyi Biotec GmbH, Bergisch Gladbach, Germany) was supplemented with 1 mM glutamine. The initial cell density was 1 Mio/ml. At the time of feed addition at t=73.7 h, the reactor volume had decreased to 1050 ml due to sampling. The feed consisted of 48 ml 10x concentrated medium including L-glutamine (Miltenyi Biotec GmbH, Bergisch Gladbach, Germany), raising the L-glutamine concentration by 1.45 mM. No antibiotics were used at any time.

**Assessment of cell density, growth rate (μ) and viability**

Total cell density was performed using a Z2 particle counter (Beckman Coulter, Brea, CA, USA) as described before [22], and apparent growth rate was approximated as described in Section 2.3.1 and Equation 4. Cell viabilities were assessed using an *Improved Neubauer*-Chamber.

**Quantification of cell cycle distribution using DNA staining**

Cell cycle distributions were quantified as described in Section 2.2.

**Significance analysis**

In order to decide when a measured process parameter of interest ( $i_{red}^{nmean}$, $i_{red}^{PR}$, $\mu(t)$, relative G1 content) at a given time point deviated from earlier measurements, thus signaling putative deviation of the cultivation from its "normal" behavior, a robust and simple criterion, without the need of *a priori* knowledge or calibration, was needed. It was introduced by means of computing the significance $p$ of the deviation of the $n$ most recently sampled data points in comparison to all other previously obtained points. For this purpose, a two-sided Student's t-test was pursued with $n$ of the most recent samples on one side, and $N$-$n$ previously obtained (control) samples on the other side; with $N$ denoting the total number of samples in the considered cultivation. This significance value $p$ was only computed if the average of the $n$ samples deviated in the direction of interest, i.e. an increase of $i_{red}^{nmean}$, $i_{red}^{PR}$ or relative G1 content, or decrease of $\mu(t)$; otherwise $p$ was defined as 1 (equal to no significance). If not stated otherwise, $n$=4 was used, however $n$=[2,3] were also assessed in any case. Any

variation was considered slightly significant (first threshold, indicated as yellow line) if $p<0.05$, and strongly significant (second threshold, indicated as red line) if $p<0.001$.
Obviously, the threshold for $p$ as well as $n$ and the specific choice of control samples belonging to the "control" group are subject to further optimization and adaptation to specific cultivation and sampling protocols in the future.

**Amino acid analytics**

Amino acids quantification was conducted by the central lab for chemical analytics, Hamburg University of Technology. In short, reversed-phase-chromatography with fluorometric detection after protein precipitation and pre-column derivatization with o-phthaldialdehyde (OPA) was employed. The setup is a combination of auto sampler, quaternary pump, degasser and a temperature controlled column compartment (Agilent, Santa Clara, CA, USA), a 250 x 4,6 mm Ultrasphere column (Beckman Coulter, Brea, CA, USA), FP1520 detector (JASCO, Easton, MD, USA) and Chromeleon data system (ThermoFisher, Waltham, MA, USA). Solvent A (0.05 M sodium acetate buffer, pH 6.5/methanol/tetrahydrofuran 84/15/1) and Solvent B (0.05 M sodium acetate buffer, pH 6.0/methanol 20/80) were used to create a gradient.

## 3 Results and Discussion

### 3.1 Generation of two novel FUCCI cell line derivatives

The aim of this section was to generate two derivatives of the *CHO-K1* cell line, each of them with a set of stably integrated and expressed genes for fluorescent cell cycle markers: *CHO-K1 CM*, containing mKO2-hCdt1(30/120) & mVenus-hGeminin(1/110) as well as *CHO-K1 CN* including mKO2-hCdt1(30/120) & mVenus-hGeminin(1/60). The flow cytometry data depicted in Fig. 1 represents cells expressing mVenus, mKO2, both or none of these proteins. The distribution is in line with the typical durations of the mammalian cell cycle phases (see Fig. 2). Based on lentiviral transduction and life cell sorting procedures it can be concluded that each cell is capable of alternating between mKO2 and mVenus fluorescence, which are for the sake of simplicity termed "red" and "green", respectively. Despite the fact that their fluorescence properties could be more accurately denoted "orange" and "yellow-green". After the initial lentiviral transduction with both constructs, only cells highly positive for the red fluorescence were selected by life cell sorting and expanded. Subsequently the same was

conducted targeting highly green fluorescent cells. Hence, all non-transducted, as well as low expressing cells were discarded. Likewise potentially existing cells with deregulated, permanent protein expression were excluded, since only single positive cells were selected in each step.

Note that the cultures are maintained polyclonal in order to preserve genetic variability for later clone selection.

Cells have been kept in culture for one month (37 days) and re-analyzed by flow cytometry to examine permanence of the marker expression. Percentages of red and/or green cells remained well within the expected range of values while the distribution pattern stayed constant, indicating stable marker expression (Fig. S3). Note, that the percentage of red and/or green cells is cell cycle depended so differences are to be expected, as an effect of different growth rates at the time of sampling. However, the constant distribution pattern documents, that the FUCCI constructs are stably integrated.

### 3.2 The fluorescence ratio $i_{red}^{n}$ as read out for cell cycle distribution

In Fig. 3, the conventionally determined cell cycle distribution of *CHO-K1 FUCCI CN* (G1[%]) versus $i_{red}^{n}$ is depicted for two independent elutriation experiments and the exponential growth phase of a (non-synchronized) bioreactor cultivation. Both elutriation experiments exhibit a linear correlation of $i_{red}^{n}$ versus the relative G1 [%] (Pearson correlation coefficients of 0.961 and 0.954, respectively); the corresponding slopes (0.808±0.116 vs. 0.726±0.072) cannot be distinguished since the difference between both experiments is smaller than their standard deviations.

The data of the bioreactor experiment represents non-synchronized growth during the uninhibited growth phase. The average G1 percentage is (59.8 ± 3.0) %. The corresponding average $i_{red}^{n}$ values are (43.6 ± 3.5) %. Accordingly, these values are in line with the elutriation data and indicate no strong variation, as expected under uninhibited conditions.

For extremely high G1 fractions, the linear correlation was less clear. This may be due to the uncertainty of classical cell cycle determination based on DNA staining, since the second (G2) peak does not appear and a quantification of G1 versus all other cells is very inaccurate.

Summarized, $i_{red}^{n}$ is a reliable and well-correlated read out of the cell cycle state of exponentially (uninhibited) growing cells without the need of additional staining or sample preparation.

Note that the other fluorescence readouts (expressed as $i_{red}^{nmean}$ or $i_{red}^{PR}$) are also a suitable representation of the cell cycle state. However, their relationship is not linear (data not shown). This is presumably caused by the different fluorescence properties of mKO2 and mVenus as well as their expression levels and sub-cellular localization.

### 3.3 $i_{red}^{nmean}$ and $i_{red}^{PR}$ as indicators of growth behavior and limitation

In this section, the relationship between the fluorescence ratio (based on two methods of detection: $i_{red}^{nmean}$ and $i_{red}^{PR}$) and the variations of growth rate (μ) due to growth inhibition are discussed. Data was generated using shaking flask experiments as well as a VSF 2000 stirred tank bioreactor.

#### Shaking flask experiments

In this section, normalized fluorescence based on plate reader measurements ($i_{red}^{PR}$) was used, since it approximates the type of data generated from on-line fluorescence probes. The experiment was performed in shaking flasks.

The curves of the apparent growth rates (μ) of *CHO-K1 FUCCI CM* and *CHO-K1 FUCCI CN* (Fig. 4) exhibit a classical batch pattern, as far as the measurement accuracy permits. Meanwhile, $i_{red}^{PR}$ displays an inverted behavior. While the growth rate increases (phases I & II), $i_{red}^{PR}$ decreases. In phase III both cultures exhibit maximum growth rate, accompanied by minimal $i_{red}^{PR}$ values. In this state, all cells proliferate at maximum speed ($\mu=\mu_{max}$), accordingly a low percentage of cells is "red".

The difference of $i_{red}^{PR}$ values during exponential growth when comparing *CHO-K1 FUCCI CM* and *CHO-K1 FUCCI CN* is a result of the subcellular localization of the fluorescent proteins. Due to its smaller size, the FUCCI protein "N" (mVenus-hGeminin(1/60)) can enter the cytoplasm, while the FUCCI protein "M" (mVenus-hGeminin(1/110)) is restrained to the nucleus. Accordingly, the latter generates lower "green" fluorescence intensities. This in turn causes higher $i_{red}^{PR}$ ratios.

Starting from phase IV, the growth rates of both cultures decrease. Simultaneously, $i_{red}^{PR}$ increases. This may be in line with previous studies which reported reduced growth rates to be associated with increased percentages of cells in G1 based on the fact that the transition of cells from late G1 to S phase is tightly controlled by nutrient availability [3–5].

This general relation has been repeatedly observed, however it does not allow for the determination of a general linear correlation covering all growth and decay phases. The Pearson correlation coefficients between $i_{red}^{PR}$ and μ(t) within either growth or decay phases ranged between -0.893 and -0.971, indicating a negative relation and partially linear correlation. However, for full cultivations and/or between different cultivations, no such linear relation has yet been obtained.

Summarized, it shows that simple total fluorescence measurements yields qualitative information about the growth behavior of FUCCI expressing cell lines, i.e. it provides reliable trends of growth rate increases and decreases.

**Detection of glutamine limitations**

Based on the previously cited putative relationship between nutrient limitation and increased G1 [5], it was hypothesized that nutrient or growth limitation may be directly detectable using the fluorescence read-out.

In order to evaluate this, glutamine limitation experiments in shaking flask cultivations using *CHO-K1 FUCCI CN* were performed. The results are illustrated in Fig. 5. The preculture and the culture including L-glutamine (culture 1) are characterized by steadily increasing cell densities until growth slows down at around 80 h of cultivation. Accordingly, $i_{red}^{PR}$ values are low and increase towards the end of the culture. Much in contrast, L-glutamine limitation (culture 2) shows inhibited growth, which is accompanied by a steep increase of $i_{red}^{PR}$. Notably, subsequent addition of L-glutamine (culture 3) restored growth and drastically lowered $i_{red}^{PR}$.

Summarized, it was confirmed that growth of the cultures was clearly L-glutamine dependent. Furthermore, growth limitations due to L-glutamine depletion are associated with high $i_{red}^{PR}$ values and *vice versa*, which also holds true after re-feeding.

**Detection of growth inhibitions in a VSF 2000 bioreactor**

In this experiment using *CHO-K1 FUCCI CN*, $i_{red}^{PR}$ values were measured as described above. Additionally, a *CytoFlex* flow cytometer was used to detect the fluorescence. The flow cytometer based total fluorescence ratio ($i_{red}^{nmean}$) was calculated to mimic the total fluorescence signal obtainable from the plate reader as well as potential florescence probes. However, possible background fluorescence of the cell culture medium caused by leaked fluorescent proteins, detectable by fluorescent probes, is omitted.

The measured total and viable cell densities values are depicted in Fig. 6; the time course of the most important amino acid concentrations (Gln, Glu, Asp) and their specific consumption rates are provided in Fig. 7. The other amino acids were also measured and are supplied in the supplementary data Fig S2.

This cultivation was divided into the following phases (transition times set approximately): Phase 0 (0h≤t<24 h) which is considered the adaptation time or lag phase; Phase 1 (24h≤t<48 h) with maximum growth rate and no limitations; Phase 2 (48h≤t<73 h) with partial limitation due to glutamine depletion; this phase included a phase 2b (59h≤t<66 h) with intermediate oxygen depletion (DO<10%); Phase 3 (73h≤t<90 h) with re-fed glutamine and other nutrients; Phase 4 (90h≤t) with re-depletion of several nutrients and rapid dying.

From Fig. 7 it can be seen that all amino acid concentration decrease throughout the cultivation at different speeds. Directly after the addition of the feed, all values display a spike, followed by decline as expected. In Fig. 7b, the consumption rates per Mio. cells for each amino acid are plotted; in Fig. 7c the corresponding average values are summarized for the aforementioned cultivation phases. At the start of cultivation, glutamine consumption is the highest, but decreases while concentrations diminish. In parallel, glutamate as well as aspartic acid consumption rates increase until available concentrations lessen, too. Directly after feeding, glutamine consumption rates strongly increased, again followed by a steep decrease, while those of glutamate and aspartic acid remain low.
Considering the stated behavior in terms of the three defined culture phases (Fig 7c), the metabolic shift of the cells is even more recognizable: In line with general knowledge, mammalian cells prefer to consume glutamine but shift towards few other amino acids if availability dictates so. When glutamine availability is restored, they tend to shift back.

In Fig. 8, the apparent growth rate (μ), based on cell counts (quantified using a Z2 particle counter), is presented two-fold: In order to address the limited sampling accuracy and error propagation, the measured cell counts were subjected to low-pass filtering and resampling (σ=12h) before computation of μ(t) [24]. Based on this *a posteriori* filtered data (depicted by the thin dotted line), a partial growth limitation is detectable at approx. 50 h and a strong

limitation at approx. 96 h. Note that this is only visible after-the-fact, including all measured data and *after* the cultivation was already finished. Overlayed in Fig. 8, the approximated growth rates based on actually available data at each time point *t* (in-time) is given by linear regression of the logarithm of the last *n*=4 cell counts versus time (rhombi). This yields considerably more noisy data; furthermore variations in growth behavior can only be detected with delay. With smaller *n*, the noise increases strongly (data not shown); with larger *n*, the delay increases.

Fig. 9 displays the corresponding total fluorescence read outs $i_{red}^{PR}$ as well as $i_{red}^{nmean}$. They increase towards the end of the cultivation, indicating reduced growth rates ($\mu$). Both $i_{red}$ values are very similar and can be fitted to a linear equation (y=mx+n) with m=1.073±0.073 and n=0.015±0.019 as can also be seen in Fig. S1, showing a high correlation (PCC=0,961) over a wide range of values with only one outlier, the last data point, corresponding to a sample from the late dying phase (162,6 h of cultivation).
In combination with the results of the previous sections, it can be concluded that it is less important, which method is used for fluorescence detection. Any total fluorescence method, capable of determining $i_{red}^{total}$ with sufficient accuracy and specificity, can be used as real-time read out for growth rates.

Much in contrast, the conventionally obtained G1 distribution data (Fig 9) does not show any systematic pattern, despite a certain amount of fluctuation. Only the very first and last data points seem to deviate slightly.

Fig. 10 displays the significance analysis of the variations within the data shown in Fig. 9. In the case of $i_{red}^{PR}$, slightly significant changes ($p<0.05$: first threshold, indicated as yellow line) are observed at t=47-50 h, indicating partial growth limitation due to glutamine depletion; further after t~75h, indicating prolonged and increasingly severe growth limitation. Highly significant changes ($p<0.001$: second threshold, indicated as red line) subsequently followed after t~89h. Likewise, for $i_{red}^{nmean}$, they were detected after t~77h ($p<0.05$: first threshold, *n*=3) and t~95h ($p<0.001$: second threshold). On the other hand, G1 did not yield any significant changes.

Based on significance analysis of Neubauer counted (viable) cell numbers, first indications of growth limitation were observed at t~96h ($n$=3, analysis not shown), obvious growth limitation and dying (second threshold, indicated as red line) was only visible at t>100 h. With Z2 particle counter and flow cytometry counted (total) cell numbers, no significant trend change was observed at all, presumably due to the inclusion of dead cells (Z2 particle counter) and due to the flow cytometry staining protocols which were not optimized for highly reproducible absolute cell number recovery.

The dissolved oxygen was as well monitored during the cultivation and aeration was adapted automatically in order to maintain desired DO (data not shown). A first trend change of aeration, indicating varying oxygen uptake rate, can be depicted retrospectively and visually at t~85 h.

During a limited time of partial oxygen depletion (DO<10%), ranging from t~59h to t~66h post bioreactor inoculation, the $i_{red}$ signals also showed a very significant deviation, this time below the normal level (analysis not shown). Very high significance for such deviation ($p<0.001$, n=2) was detected for t~66 h. It remains to be seen whether such a signal provides additional information for the purpose of process monitoring and control compared to conventionally measured DO probe signal.

From these results it can be concluded that detection of the total fluorescence ratios $i_{red}^{nmean}$ and $i_{red}^{n}$ in combination with a standardized significance analysis is capable of detecting inhibitions of growth many hours – in our case at least 19 h – earlier compared to classical cell density based approaches. Also partial growth limitations, adaptation phases and oxygen depletions can be observed with reasonable significance given the limited amount of samples used.

A more detailed consideration of the differences between $i_{red}^{nmean}$ and $i_{red}^{n}$ leads to the conclusion that different time points of significance detection are related to the amount of available data points, rather than the type of total fluorescence detection method. Hence, sampling frequency is key to detect significant changes earlier and more reliably. The presented data is still limited by the manual sampling method and the required hands on time.

Herein lies the prime potential of the method: Online or at-line probe based monitoring of the total fluorescence ratio ($i_{red}$) can easily be executed and analyzed in minutes to seconds.

**Conclusion**

In this study, the first adaptation of the Fluorescent Ubiquitination-based Cell Cycle Indicator (FUCCI) system to a production relevant cell line (CHO-K1 [1]), for the purpose of real time compatible growth monitoring is reported. Evaluation is presented based on various shaking flask and bioreactor cultivations. The two novel cell line derivatives *CHO-K1 FUCCI CM* and *CHO-K1 FUCCI CN* allow for an easy and reliable fluorescence read out which is highly correlated (PCC=0.961 and 0.954, respectively) to the cell cycle distribution and reliably indicates ongoing changes of growth rates of cell cultures. Based on these properties, the total fluorescence ratio was used to monitor the growth behavior of cultures and detect growth limitations considerably earlier and more reliably than cell density or conventional cell cycle (DNA staining) based approaches, and to some extent even earlier than with oxygen uptake rate (OUR) based online analysis.

The total fluorescence ratio has proven to be a reliable read-out. By design it is less error prone than fluorescence-per-cell-number based methods as it is self-normalized and doesn't require an additional method of cell quantification. Much in contrast, detection of the fluorescence per volume may potentially be used to approximate the cell density.

As indented by design, *CHO-K1 FUCCI CN* is capable of yielding a broader range of values compared to *CHO-K1 FUCCI CM* (see section 3.3, Fig. 4), hence *CHO-K1 FUCCI CN* was used in the bioreactor setup.

Future studies and potential industrial application would benefit from total fluorescence probes with specific filter sets in combination with automated significance analysis. However, probe and/or reactor must be designed appropriately to circumvent erroneous detection of other light sources. In principle, the stated concept is compatible with any suitable fluorescence detection system as well as fluorescent cell cycle indicator combination. However the authors would like to emphasize the importance of proper setup design and validation. While combinations of fluorescence proteins with more spectral diversity can reduce requirements for detection specificity, special diligence must be applied with regard to signal intensities caused by the fluorescent proteins stokes shift, quantum yield and related parameters. When using different light sources for excitation, intensities must be managed

carefully. In addition, the intended fluorescent protein expression levels (governed by integration site, number and promotor) should be chosen carefully, considering signal intensity requirements and metabolic burden. Hence, the intended behavior of each novel cell line derivative ought to be evaluated. Finally, a more in depth investigation of possible interdependencies between the fluorescence read out and other process parameters, such as pH and temperature, under production processes conditions is advisable.

## 5 References


1. Jayapal K, Wlaschin K, Hu W-S, Yap M. Recombinant Protein Therapeutics from Cho Cells - 20 Years and Counting. *CHO Consort SBE Spec Ed*. 2007:40-47. http://www.aiche.org/sites/default/files/docs/pages/CHO.pdf. Accessed May 26, 2016.
2. Biechele P, Busse C, Solle D, Scheper T, Reardon K. Sensor systems for bioprocess monitoring. *Eng Life Sci*. 2015;15(5):469-488. doi:10.1002/elsc.201500014.
3. Sitton G, Srienc F. Mammalian cell culture scale-up and fed-batch control using automated flow cytometry. *J Biotechnol*. 2008;135(2):174-180. doi:10.1016/j.jbiotec.2008.03.019.
4. Kuystermans D, Mohd A, Al-Rubeai M. Automated flow cytometry for monitoring CHO cell cultures. *Methods*. 2012;56(3):358-365. doi:10.1016/j.ymeth.2012.03.001.
5. Saqcena M, Menon D, Patel D, Mukhopadhyay S, Chow V, Foster DA. Amino acids and mTOR mediate distinct metabolic checkpoints in mammalian G1 cell cycle. *PLoS One*. 2013;8(8):e74157. doi:10.1371/journal.pone.0074157.
6. Sakaue-Sawano A, Kurokawa H, Morimura T, Hanyu A, Hama H, Osawa H, Kashiwagi S, Fukami K, Miyata T, Miyoshi H, Imamura T, Ogawa M, Masai H, Miyawaki A. Visualizing spatiotemporal dynamics of multicellular cell-cycle progression. *Cell*. 2008;132(3):487-498. doi:10.1016/j.cell.2007.12.033.
7. Sakaue-Sawano A, Ohtawa K, Hama H, Kawano M, Ogawa M, Miyawaki A. Tracing the silhouette of individual cells in S/G2/M phases with fluorescence. *Chem Biol*. 2008;15(12):1243-1248. doi:10.1016/j.chembiol.2008.10.015.
8. Fukuhara S, Zhang J, Yuge S, Ando K, Wakayama Y, Sakaue-Sawano A, Miyawaki A, Mochizuki N. Visualizing the cell-cycle progression of endothelial cells in zebrafish. *Dev Biol*. 2014;393(1):10-23. doi:10.1016/j.ydbio.2014.06.015.
9. Hama H, Kurokawa H, Kawano H, Ando R, Shimogori T, Noda H, Fukami K, Sakaue-Sawano A, Miyawaki A. Scale: a chemical approach for fluorescence imaging and reconstruction of transparent mouse brain. *Nat Neurosci*. 2011;14(11):1481-1488. doi:10.1038/nn.2928.
10. Horie T, Shinki R, Ogura Y, Kusakabe TG, Satoh N, Sasakura Y. Ependymal cells of chordate larvae are stem-like cells that form the adult nervous system. *Nature*. 2011;469(7331):525-528. doi:10.1038/nature09631.
11. Makhijani K, Alexander B, Tanaka T, Rulifson E, Brückner K. The peripheral nervous system supports blood cell homing and survival in the Drosophila larva. *Development*. 2011;138(24):5379-5391. doi:10.1242/dev.067322.
12. Dan S, Okamura M, Mukai Y, Yoshimi H, Inoue Y, Hanyu A, Sakaue-Sawano A, Imamura T, Miyawaki A, Yamori T. ZSTK474, a specific phosphatidylinositol 3-kinase inhibitor, induces G1 arrest of the cell cycle in vivo. *Eur J Cancer*. 2012;48(6):936-943. doi:10.1016/j.ejca.2011.10.006.

13. Sakaue-Sawano A, Kobayashi T, Ohtawa K, Miyawaki A. Drug-induced cell cycle modulation leading to cell-cycle arrest, nuclear mis-segregation, or endoreplication. *BMC Cell Biol*. 2011;12:2. doi:10.1186/1471-2121-12-2.
14. Miwa S, Yano S, Kimura H, Yamamoto M, Toneri M, Matsumoto Y, Uehara F, Hiroshima Y, Murakami T, Hayashi K, Yamamoto N, Bouvet M, Fujiwara T, Tsuchiya H, Hoffman RM. Cell-cycle fate-monitoring distinguishes individual chemosensitive and chemoresistant cancer cells in drug-treated heterogeneous populations demonstrated by real-time fucci imaging. *Cell Cycle*. 2015;14(4):621-629. doi:10.4161/15384101.2014.991604.
15. Yano S, Zhang Y, Miwa S, Tome Y, Hiroshima Y, Uehara F, Yamamoto M, Suetsugu A, Kishimoto H, Tazawa H, Zhao M, Bouvet M, Fujiwara T, Hoffman RM. Spatial-temporal FUCCI imaging of each cell in a tumor demonstrates locational dependence of cell cycle dynamics and chemoresponsiveness. *Cell Cycle*. 2014;13(13):2110-2119. doi:10.4161/cc.29156.
16. Miwa S, Yano S, Tome Y, Sugimoto N, Hiroshima Y, Uehara F, Mii S, Kimura H, Hayashi K, Efimova E V., Fujiwara T, Tsuchiya H, Hoffman RM. Dynamic color-coded fluorescence imaging of the cell-cycle phase, mitosis, and apoptosis demonstrates how caffeine modulates cisplatinum efficacy. *J Cell Biochem*. 2013;114(11):2454-2460. doi:10.1002/jcb.24593.
17. Zhang L, Wu C, Bouvet M, Yano S, Hoffman RM. Traditional Chinese medicine herbal mixture LQ arrests FUCCI-expressing HeLa cells in G 0 / G 1 phase in 2D plastic ,. *Oncotarget*. 2015;6(7):5292-5298. doi:10.18632/oncotarget.2983.
18. Yano S, Li S, Han Q, Tan Y, Bouvet M, Fujiwara T, Hoffman RM. Selective methioninase-induced trap of cancer cells in S/G2 phase visualized by FUCCI imaging confers chemosensitivity. *Oncotarget*. 2014;5(18):8729-8736. doi:10.18632/oncotarget.2369.
19. Kostyrko K, Bosshard S, Urban Z, Mermod N. A role for homologous recombination proteins in cell cycle regulation. *Cell Cycle*. 2015;14(17):2853-2861. doi:10.1080/15384101.2015.1049784.
20. Zielke N, Edgar BA. FUCCI sensors: powerful new tools for analysis of cell proliferation. *Wiley Interdiscip Rev Dev Biol*. 2015;4(5):469-487. doi:10.1002/wdev.189.
21. Weber K, Bartsch U, Stocking C, Fehse B. A multicolor panel of novel lentiviral "gene ontology" (LeGO) vectors for functional gene analysis. *Mol Ther*. 2008;16(4):698-706. doi:10.1038/mt.2008.6.
22. Castillo Salvador A-E, Fuge G, Jandt U, Zeng A-P. Growth kinetics and validation of near-physiologically synchronized HEK293S Cultures. *Eng Life Sci*. 2015;15(5):509-518. doi:10.1002/elsc.201400224.
23. Kremers G-J, Gilbert SG, Cranfill PJ, Davidson MW, Piston DW. Fluorescent proteins at a glance. *J Cell Sci*. 2011;124(Pt 2):157-160. doi:10.1242/jcs.072744.
24. Jandt U, Platas Barradas O, Pörtner R, Zeng A-P. Synchronized mammalian cell culture: Part II-population ensemble modeling and analysis for development of reproducible processes. *Biotechnol Prog*. 2015;31(1):175-185. doi:10.1002/btpr.2006.

## Figure legends

**Fig 1.: Fluorescence of CHO-K1 FUCCI CM and CHO-K1 FUCCI CN analyzed in flow cytometer** Cultures of the novel cell line derivatives display single positive, double positive and double negative FUCCI protein expression.

**Fig 2.: Cell cycle regulation and FUCCI.** Cells indicating their individual cell cycle phase by fluorescence. The G1 phase is associated with "red" mKO2 fluorescence; S, G2 and M phases with "green" mVenus fluorescence. During G1 to S phase transition, cells are double positive, during and directly after mitosis double negative.

**Fig 3.: Correlation of $i_{red}^{n}$ and G1 [%] – threshold based** The data points of both elutriation runs exhibit a linear correlation with the relative G1 fraction. Both slopes (Elutriation Exp. A and B) are indistinguishable, considering measurement accuracy. The corresponding distribution in the non-synchronized bioreactor experiment during its non-growth-limited phases (average G1 at (59.8 ± 3.0) %; average $i_{red}^{n}$ (43.6 ± 3.5) %) is in line with the elutriation data.

**Fig 4.: Visualization of $i_{red}^{PR}$ distribution vs. apparent growth rate (μ) in shaking flask experiments without limitations.** Top: *CHO-K1 FUCCI CM*; bottom: *CHO-K1 FUCCI CN.* The growth rate μ exhibits the classical batch growth pattern: Starting with a lag (I) and acceleration phase (II), followed by exponential growth (III), deceleration (IV), stationary phase (V) and finally the death phase (VI). The horizontal error bars indicate the width of the Gaussian filter (σ=6 h). The $i_{red}^{PR}$ values display a qualitatively inverted behavior. The error bars indicate the standard deviation of the technical triplicates. Pearson coefficients indicate a negative relationship but are not accurate enough to support negative correlation for all growth phases (CM I and II -0.956, IV to VI -0.893; CN I and II -0.936, IV to VI -0.971).

**Fig 5.: $i_{red}^{PR}$ dependency on nutrient limitation**
Illustration of behavior of growth and fluorescence readout, depending on depletion and re-availability of L-glutamine (Gln). The upper graph illustrates that increase in cell density depends on availability of Gln: In case of culture 1, Gln was available from the beginning, in case of culture 3, Gln has been added by splitting culture 2 equally. The lower graph confirms L-glutamine limitation to be associated with high $i_{red}^{PR}$ values.

**Fig 6.: Total cell density [Mio/ml] and viability [%]** Cell densities increase until around 95 h of cultivation, subsequently they decrease. Accordingly, viabilities decrease rapidly towards the end of the culture.

**Fig 7.: a) Amino acid concentrations (AA), b) their consumption rates over time per Mio cells (dAA/dX) as well as c) grouped into three distinct cultivation phases (defined in the text).** Amino acid consumption appears to be governed by availability. Cells prefer glutamine over glutamate and aspartic acid.

**Fig 8.: Growth rate during cultivation** The growth rate was calculated based on particle counter data (Z2, Beckman Coulter), both in-time with a 4-point sliding average approach (rhombi), and *a posteriori* after low-pass filtering and re-sampling (σ=12h) before computation of μ(t) [24] (thin dotted line).

**Fig 9.: Comparison of $i_{red}^{PR}$ and $i_{red}^{nmean}$as well as the G1 [%].** While $i_{red}^{PR}$ and $i_{red}^{nmean}$ increase towards the end of the culture, G1 distribution displays no systematic variation.

**Fig 10.: Significance analysis of $i_{red}^{PR}$ and $i_{red}^{nmean}$ as well as G1 [%].** $i_{red}^{PR}$ based analysis indicates slightly significant changes ($p<0.05$: first threshold, yellow line) at t=47-50 h, and t~75h. Highly significant changes ($p<0.001$: second threshold, indicated as red line) after t~89h. For $i_{red}^{nmean}$, slightly significant changes after t~77h ($p<0.05$: first threshold) and highly significant changes ($p<0.001$: second threshold) after t~95h. G1 [%] analysis did not yield values above significance levels.

**Fig 11.: Correlation of $i_{red}^{PR}$ and $i_{red}^{nmean}$bioreactor cultivation** Both values are calculated based on total fluorescence data, obtained using different analytical devices (plate reader and CytoFlex flow cytometer) and sample preparation protocols (viable cells vs. cells stored in EtOH). The data can be fitted to a linear equation (y=mx+n) with m=1.073±0.073 and n=0.015±0.019. PCC=0.961. The last data point, corresponding to a sample from the late dying phase (162,6 h of cultivation) was excluded as outlier.

**Fig S2.: Amino acid concentrations** Changes over time display the same behavior described above. Depletion of amino acids, preferred for catabolism (48 – 73 h), increase by feed (73 h) and re-depletion (>73 h).

**Fig S3.:** Flow cytometric analysis of CHO cells expressing FUCCI proteins to examine stability of the marker expression. The analysis was carried out at two separate time points after transduction with two FUCCI-protein expressing lentiviral vectors. A) CHO cells analyzed 3 days after transduction. B) CHO cells analyzed 40 days after transduction.

**Fig S4.:** Exponentially growing CHO-K1 FUCCI CN culture Upper image: Overview, lower panel (from left to right): S/G2/M pase; G1 phase, and G1 to S phase transition as indicated in the over view, magnified.

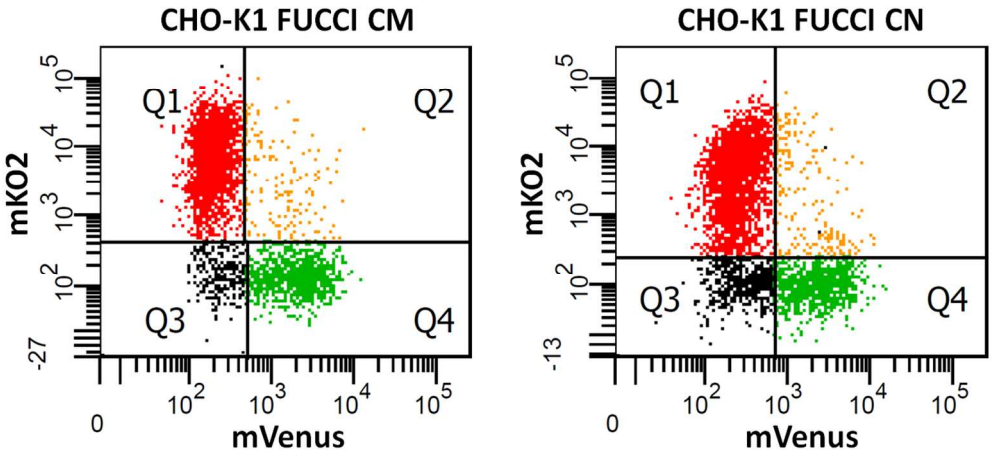


Fluorescence of CHO K1 FUCCI CM and CHO K1 FUCCI CN analyzed in flow cytometer Cultures of the novel cell line derivatives display single positive, double positive and double negative FUCCI protein expression.

119x55mm (300 x 300 DPI)

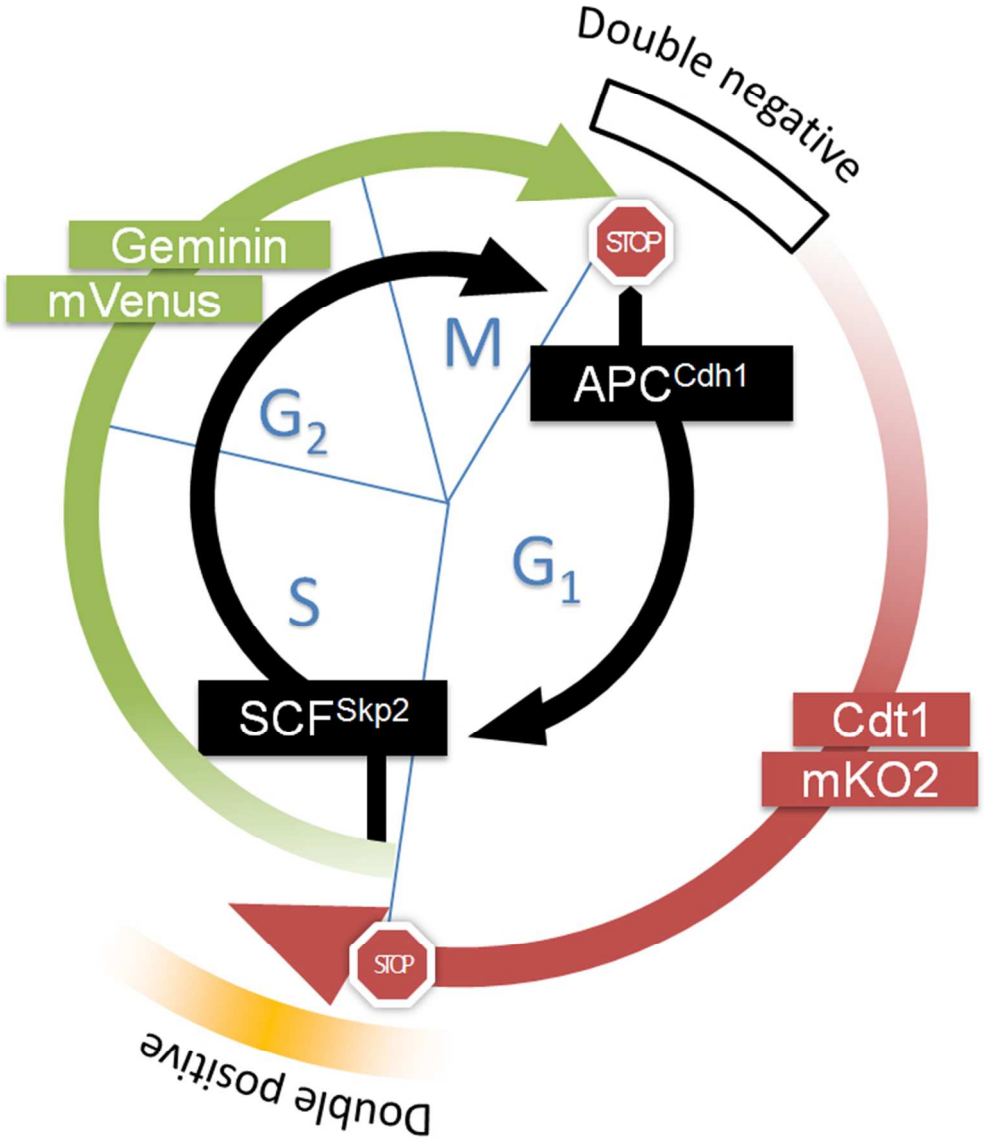


Cell cycle regulation and FUCCI. Cells indicating their individual cell cycle phase by fluorescence. The G1 phase is associated with "red" mKO2 fluorescence; S, G2 and M phases with "green" mVenus fluorescence. During G1 to S phase transition, cells are double positive, during and directly after mitosis double negative.

62x72mm (300 x 300 DPI)

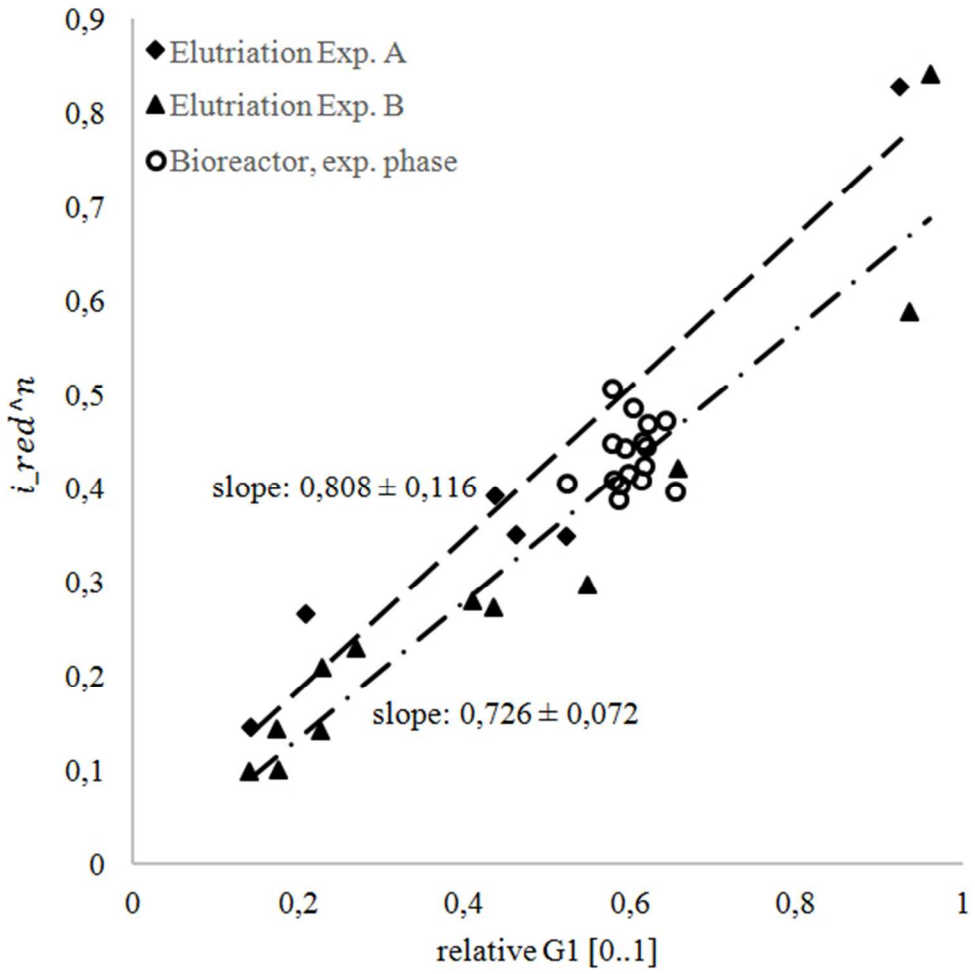


Correlation of i_red^n and G1 [%] – threshold based The data points of both elutriation runs exhibit a linear correlation with the relative G1 fraction. Both slopes (Elutriation Exp. A and B) are indistinguishable, considering measurement accuracy. The corresponding distribution in the non-synchronized bioreactor experiment during its non-growth-limited phases (average G1 at (59.8 ± 3.0) %; average i_red^n (43.6 ± 3.5) %) is in line with the elutriation data.

52x52mm (300 x 300 DPI)

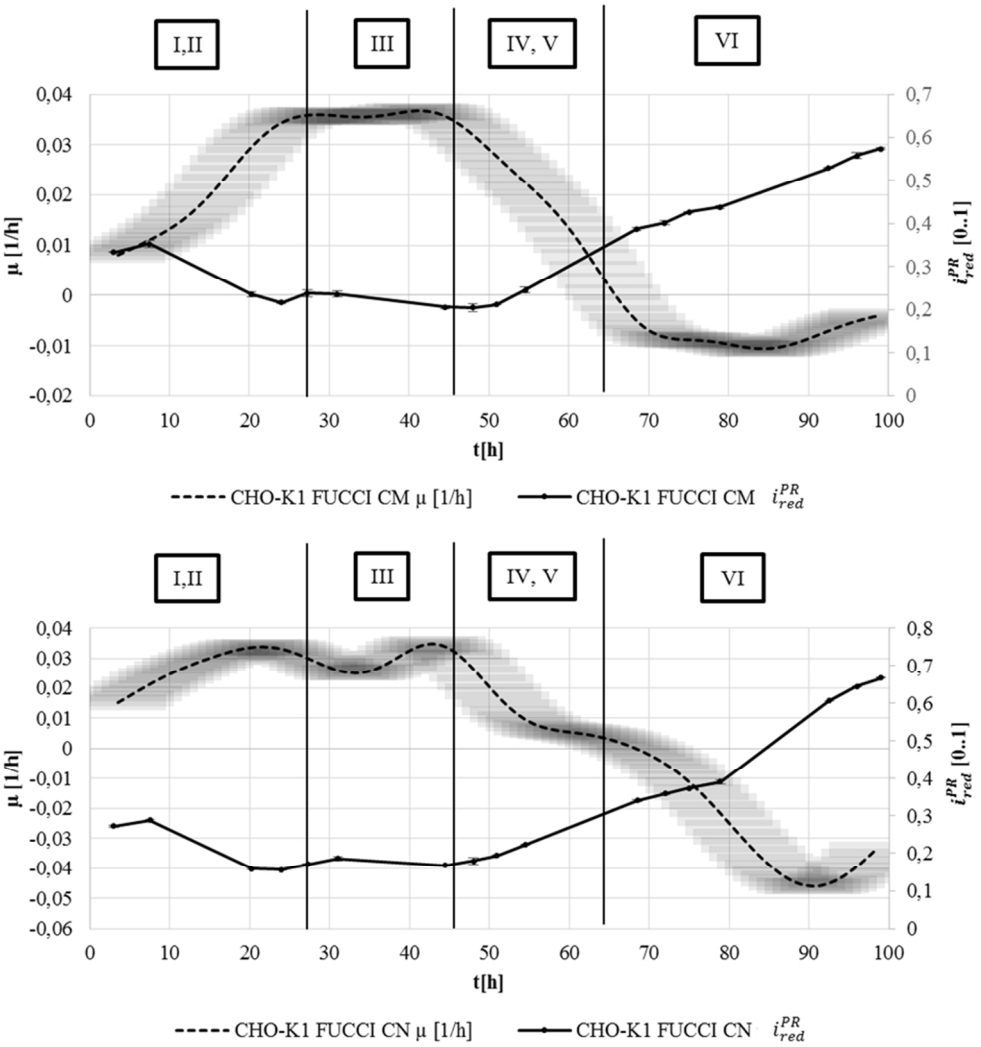


Visualization of i_red^PR distribution vs. apparent growth rate (μ) in shaking flask experiments without limitations.
Top: CHO-K1 FUCCI CM; bottom: CHO-K1 FUCCI CN. The growth rate μ exhibits the classical batch growth pattern: Starting with a lag (I) and acceleration phase (II), followed by exponential growth (III), deceleration (IV), stationary phase (V) and finally the death phase (VI). The horizontal error bars indicate the width of the Gaussian filter (σ=6 h). The i_red^PR values display a qualitatively inverted behavior. The error bars indicate the standard deviation of the technical triplicates. Pearson coefficients indicate a negative relationship but are not accurate enough to support negative correlation for all growth phases (CM I and II -0.956, IV to VI -0.893; CN I and II -0.936, IV to VI -0.971).

82x88mm (300 x 300 DPI)

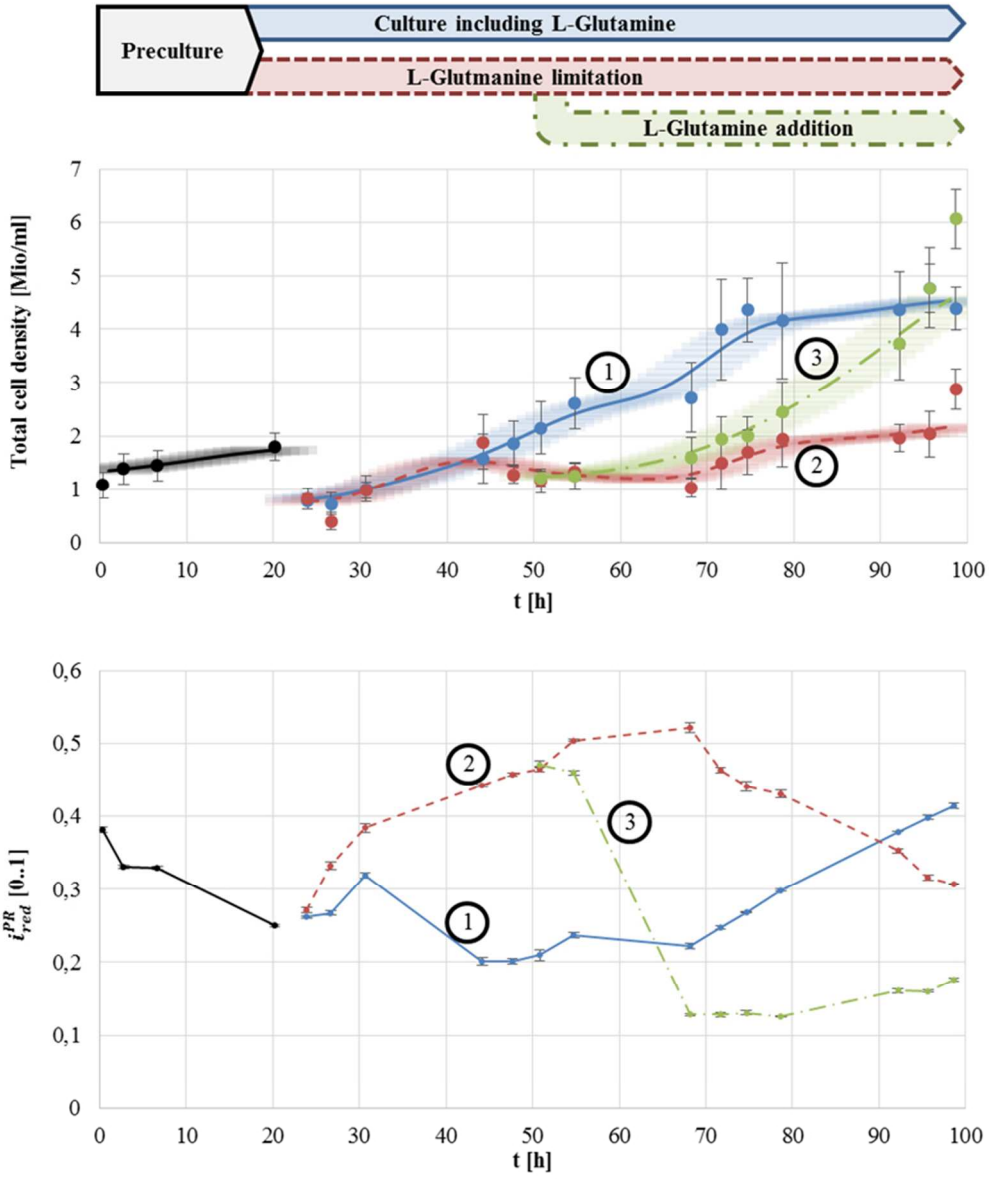


i_red^PR dependency on nutrient limitation
Illustration of behavior of growth and fluorescence readout, depending on depletion and re-availability of L-glutamine (Gln). The upper graph illustrates that increase in cell density depends on availability of Gln: In case of culture 1, Gln was available from the beginning, in case of culture 3, Gln has been added by splitting culture 2 equally. The lower graph confirms L-glutamine limitation to be associated with high i_red^PR values.

74x88mm (300 x 300 DPI)

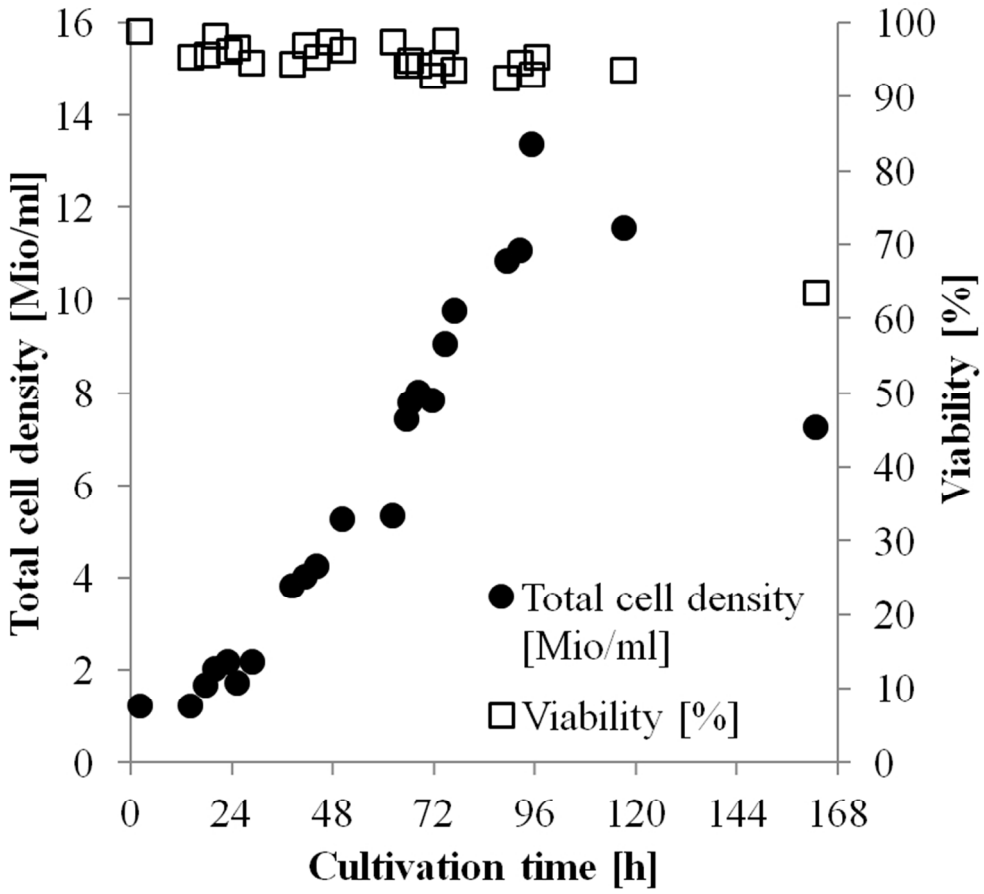


Total cell density [Mio/ml] and viability [%] Cell densities increase until around 95 h of cultivation, subsequently they decrease. Accordingly, viabilities decrease rapidly towards the end of the culture.

72x66mm (300 x 300 DPI)

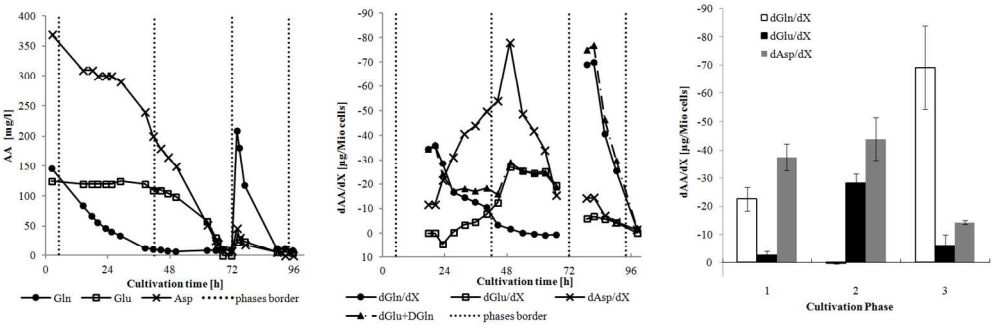


a) Amino acid concentrations (AA), b) their consumption rates over time per Mio cells (dAA/dX) as well as c) grouped into three distinct cultivation phases (defined in the text). Amino acid consumption appears to be governed by availability. Cells prefer glutamine over glutamate and aspartic acid.

146x48mm (300 x 300 DPI)

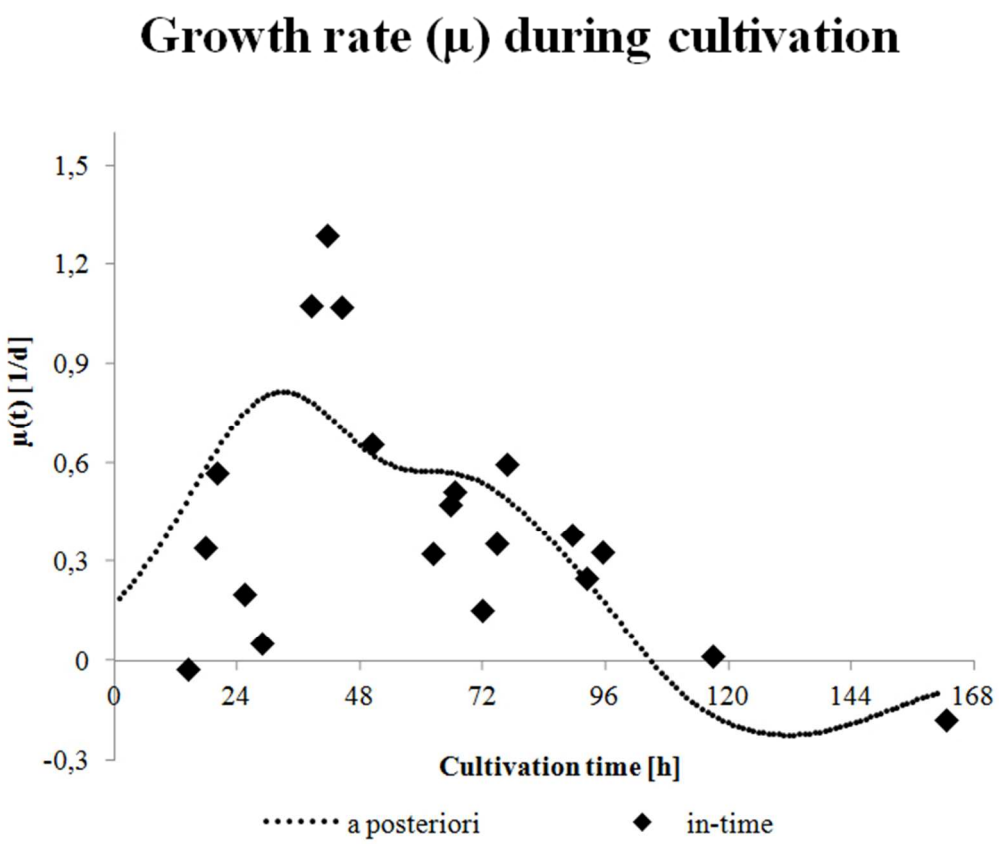


Growth rate during cultivation The growth rate was calculated based on particle counter data (Z2, Beckman Coulter), both in-time with a 4-point sliding average approach (rhombi), and a posteriori after low-pass filtering and re-sampling (σ=12h) before computation of μ(t) [17] (thin dotted line).

58x49mm (300 x 300 DPI)

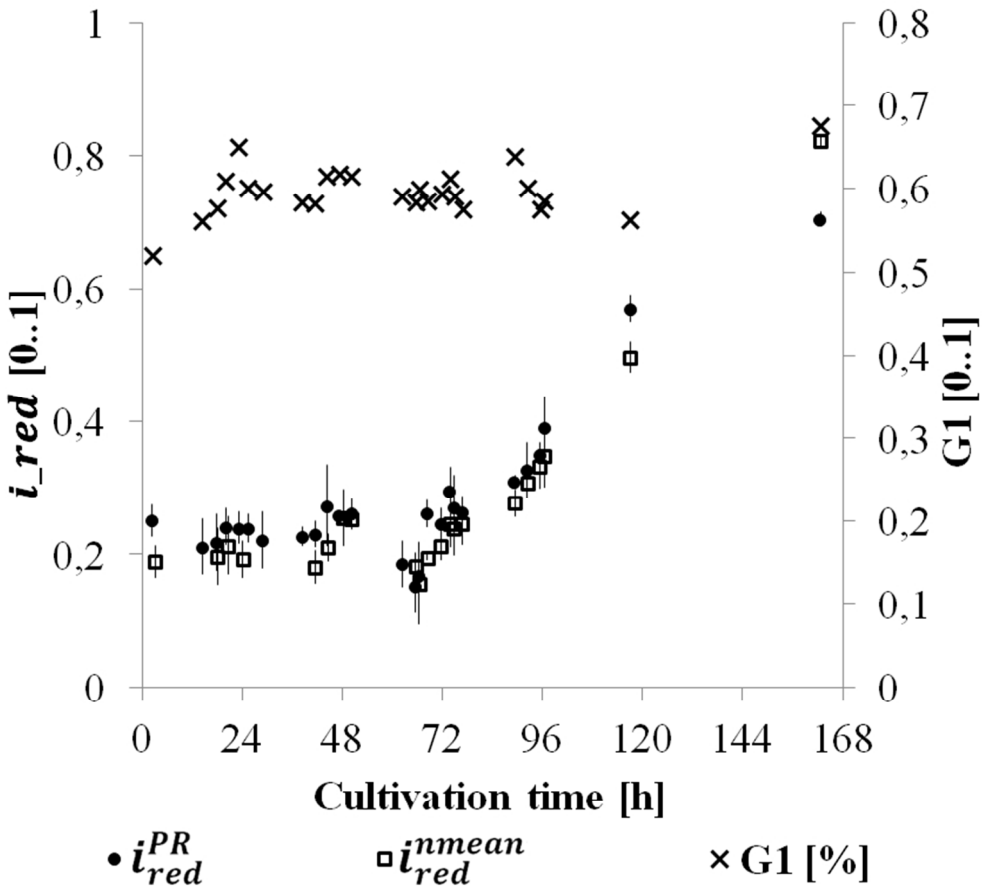


Comparison of i_red^PR and i_red^nmeanas well as the G1 [%]. While i_red^PR and i_red^nmean increase towards the end of the culture, G1 distribution displays no systematic variation.

72x65mm (300 x 300 DPI)

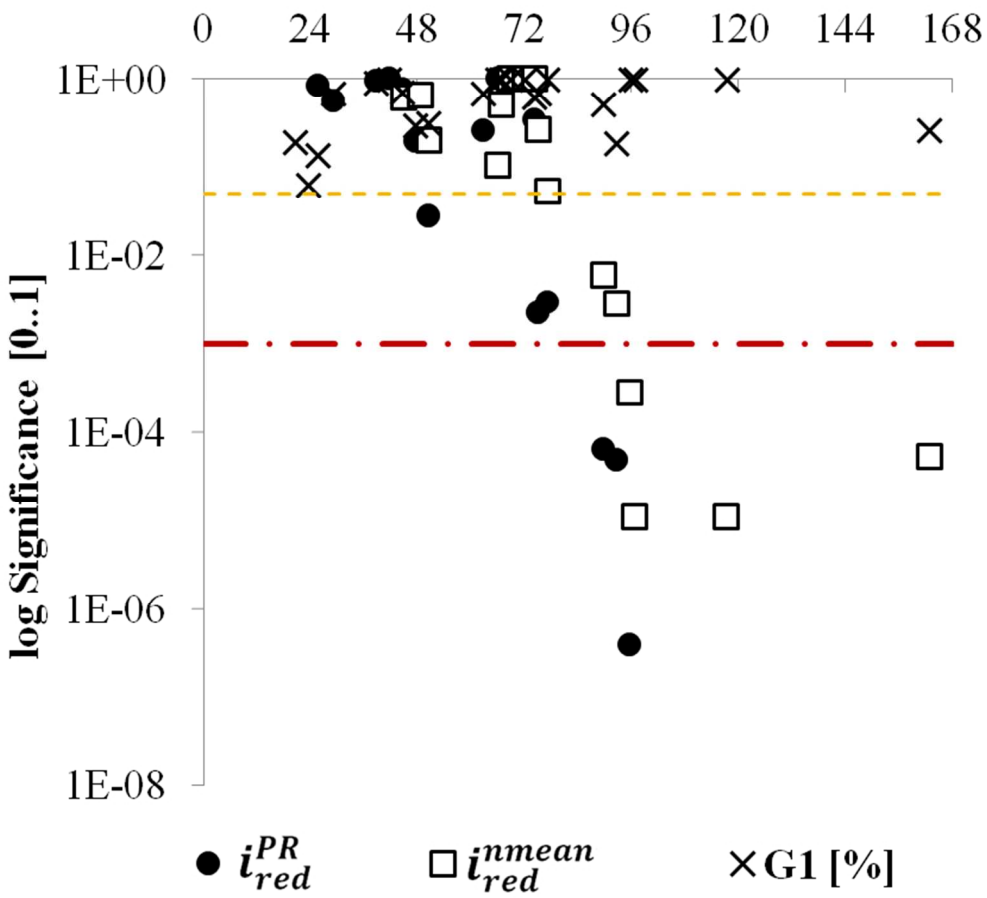


Significance analysis of i_red^PR and i_red^nmean as well as G1 [%]. i_red^PR based analysis indicates slightly significant changes ($p<0.05$: first threshold, yellow line) at t=47-50 h, and t~75h. Highly significant changes ($p<0.001$: second threshold, indicated as red line) after t~89h. For i_red^nmean, slightly significant changes after t~77h ($p<0.05$: first threshold) and highly significant changes ($p<0.001$: second threshold) after t~95h. G1 [%] analysis did not yield values above significance levels.

71x64mm (300 x 300 DPI)